Friction Identification and Compensation in Robotic Manipulators

Mehrdad R. Kermani, Rajnikant V. Patel, *Fellow, IEEE*, and Mehrdad Moallem, *Member, IEEE*

***Abstract*—In this paper, friction identification and friction compensation in the joints of a robotic manipulator are studied. The friction force is modeled using a single-state dynamic model that is utilized in the friction compensation algorithm. A new method for identifying the parameters of the aforementioned model in a robotic manipulator is presented. To evaluate the performance of this method, two different manipulators with different friction characteristics are examined. A 2-DOF manipulator that is used for high-speed micrometer precision manipulation and a 4-DOF macromanipulator that is used for long-reach positioning tasks are considered. It is shown that despite the different nature of the two manipulators, the same method can effectively improve the speed, accuracy, and smoothness of the manipulation in both cases.**

***Index Terms*—Friction compensation, friction force, identification, modeling, robotic manipulator.**

I. Introduction

FRICTION compensation can play an important role in diverse control applications. This includes applications that involve high-precision and fast motion, as well as those containing heavy and sluggish servomechanisms with slow tracking velocities. In each case, the friction force needs to be adequately identified and compensated for to improve the transient performance and reduce the steady-state tracking errors. Friction compensation also ensures a smooth control signal without resorting to high feedback gains.

The difficulties associated with friction compensation stem from the fact that friction force has various forms, some of which are not completely understood. Stribeck, stiction, and sliding forces are among such forms that dynamically, depending on the time, position, and velocity, characterize the friction force. Thus, obtaining a model that can embody all such characteristics of the friction force is not an easy task. In this regard, many researchers have studied this phenomenon and suggested a number of models. Dahl was the first to present a systematic model for Coulomb and sliding friction [7]. This model has been widely used for dynamic and adaptive friction compensation by other researchers [4]. A dynamic model of friction was proposed by Olsson *et al.* [15]. The model, which is also known as the LuGre model, incorporates a single continuous state to model presliding displacement. The model describes the behavior of elastic *bristles* as a function of relative velocity between two surfaces. This idea was first adopted by Haessing and Friedland [9] to visualize the contact behaviors of two surfaces at a microscopic level using elastic bristles. Leonard and Krishnaprasad [8] studied an adaptive model of friction for low-velocity position tracking systems. A new dynamical model of friction, which allowed accurate modeling both in the sliding and presliding regimes, was proposed in [17]. Each of these models may pertain to a particular application, and selecting an appropriate model for a given application is not trivial. A comprehensive literature review on this subject is given in [1].

Having selected an appropriate model, the parameters of the model are needed to be experimentally identified to implement the model. Friction identification is another challenging part of the friction compensation process. It can be achieved either offline or online as part of a system's operation. In offline identification, the motion through which the data are gathered can be deliberately specified. Online identification must use data from normal system operations. In this paper, offline identification is studied, and a practical method for measuring the parameters of the friction force is presented. This method is particularly adequate for robotic manipulators. It is shown that a dynamic model of friction force, which is identified using initial measurements, can result in very accurate motion control without the necessity of resorting to high feedback gains.

The main motivation for this paper arose from unsuccessful attempts at controlling industrial manipulators to a certain degree of accuracy. Friction can cause more than 50% error in some heavy industrial manipulators, while any changes in control parameters to improve the performance of the systems is usually unsuccessful. Adding a steady-state model of friction can alleviate the problem to a certain extent. The final remedy for this problem involves utilizing a dynamic model of the friction force. However, the suggested methods of identifying model parameters in the current literature [5], [11] are not feasible for robotic manipulators. Most robotic manipulators have a limited workspace that prohibits running their joints at a certain constant velocity as required by the suggested methods. Thus, a new method of identifying such parameters in a robotic manipulator whose joint friction is modeled as in [6] is suggested. The method only requires the application of a low-frequency sinusoidal torque to each joint individually.

The organization of this paper is given as follows: In Section II, a dynamic model of friction force is studied. In

Manuscript received March 25, 2005; revised August 21, 2007. This work was supported in part by the Natural Sciences and Engineering Research Council of Canada under Grant STPGP215729-98, Grant RGPIN1345, and Grant RGPIN227612.

M. R. Kermani and R. V. Patel are with the Department of Electrical and Computer Engineering, University of Western Ontario, London, ON N6A 5B8, Canada, and also with the Canadian Surgical Technologies and Advanced Robotics, London, ON N6A 5A5, Canada.

M. Moallem is with the School of Engineering Science, Simon Fraser University, Burnaby, BC V5A 1S6, Canada.

Color versions of one or more of the figures in this paper are available online at http://ieeexplore.ieee.org.

Digital Object Identifier 10.1109/TIM.2007.907957

Section III, a generalized method for measuring friction force in robotic manipulators is discussed. Finally, in Section IV, experimental results are presented for two different types of manipulators.

II. Modeling

Consider the following dynamics of a robotic manipulator with n joints:

$$M(q)\ddot{q} + c(q,\dot{q})\dot{q} + g(q) = \tau - \tau_F \tag{1}$$

where $q = (q_1, q_2, \ldots, q_n)^T$ is the joint angle vector, $M(q)$ is the mass matrix, $c(q,\dot{q})\dot{q}$ is the Coriolis and centrifugal term, $g(q)$ is the gravity term, and τ and τ_F are the vectors of applied forces/torques and the friction forces/torques, respectively. Henceforth, the term force is used for referring to both force and torque. The friction force at each joint, e.g., joint j of the manipulator, can be dynamically modeled as a function of joint velocity as follows [6]:

$$\begin{aligned} \dot{z} &= \dot{q}_j - \frac{\sigma_0|\dot{q}_j|}{s(\dot{q}_j)}z \\ \tau_{F_j} &= \sigma_1\dot{z} + \sigma_0 z + \sigma_2\dot{q}_j \end{aligned} \tag{2}$$

where z is the average deflection of some fictitious bristles that cause friction between the two surfaces (see [6] for the detailed description of the bristles), τ_{F_j} is the joint j friction force, σ_0 and σ_1 are the stiffness and damping coefficients, respectively, σ_2 is the viscous coefficient, and $s(\dot{q}_j)$ is a scalar function given by

$$s(\dot{q}_j) = F_c + (F_s - F_c)e^{-\alpha|\dot{q}_j|}. \tag{3}$$

In (3), F_c is the Coulomb force, F_s is the stiction force, and α determines the variation of $s(\dot{q}_j)$ between F_s and F_c. As can be observed, the friction force is characterized by six parameters, namely F_c, F_s, σ_0, σ_1, σ_2, and α, from which F_c, F_s, and α describe the steady-state part of the model. Moreover, σ_0 specifies the stiffness property of the friction force and is a positive number, whereas σ_1 specifies the damping property of the friction dynamics. In a system with viscous friction, the necessary and sufficient condition for passivity [2], [14] of the model is given by $\epsilon_2 \leqslant \epsilon_1(1 + (\sigma_2/\sigma_1))$, where $\epsilon_1 = (1/s(\dot{q}_j)|_{\dot{q}_j=0})$, and $\epsilon_2 = (1/s(\dot{q}_j)|_{\dot{q}_j\to\infty})$. Here, the objective is to experimentally estimate the values of the model parameters for each joint of a manipulator.

III. Friction Identification

To model friction force in the joints of a robot, the first step is to obtain a mapping between the friction force and the joint velocity. One method proposed to this end is to run each joint of the robot at various constant velocities and obtain the corresponding friction forces [5], [11]. However, due to the limited workspace of a robotic manipulator, the proposed method is often not feasible. Thus, an alternative method in which the joint angle is kept within the manipulator's workspace is desirable. To this end, a low-frequency sinusoidal torque is applied to each joint of the manipulator, while the other joints are locked and the corresponding velocity is measured. It is worth mentioning that the amplitude and the frequency of the applied sinusoidal torque should be carefully selected. In other words, the applied torque should result in a joint velocity that is slow enough so that the joint angles remain within the manipulator's workspace during one cycle of the input signal and the Coriolis and centrifugal forces remain negligible. On the other hand, the joint velocity should become fast enough to cause a transition of the friction force from the presliding to the sliding state and to reveal the viscosity effect. In the end, with no preliminary information about the friction force, finding an appropriate torque signal is a matter of a few trials and errors.

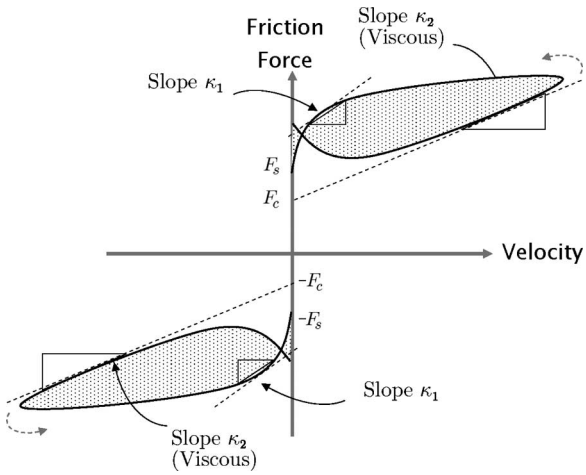

Fig. 1. Friction force/torque versus velocity.

Having measured a friction–velocity map for a joint, the parameters of the friction model given in (2) can be identified to match that joint. The same procedure will be repeated so as to obtain a friction model for each joint of the manipulator. The models obtained in this way are then utilized to estimate and compensate for the friction force during robot operations.

A. Friction–Velocity Map

Assuming that the aforementioned conditions are all satisfied, the equation of motion for each joint of the manipulator (e.g., joint j) can be rewritten as follows:

$$M_{jj}\ddot{q}_j + g_j \simeq \tau_j - \tau_{F_j} \tag{4}$$

where M_{jj} is the moment of inertia of joint j around its z-axis, $\tau_j = \tau_{m_j}\sin(\omega_j t) + g_j$ is the applied torque, and τ_{F_j} is the joint friction force. By calculating $\ddot{q}_j$ after numerical differentiation of the joint velocity and assuming perfect gravity cancelation, τ_{F_j} can be obtained from (4) as follows:

$$\tau_{F_j} \simeq \tau_{m_j}\sin(\omega_j t) - M_{jj}\ddot{q}_j. \tag{5}$$

Having obtained the friction force from (5), the values of the friction force are plotted against the joint velocities to obtain a typical friction–velocity map, as shown in Fig. 1.

When an exact mass matrix $M(q)$ is not known or its elements are not constant for different joint angles, using an approximate value of M_{jj} is inevitable. Yet, small values of

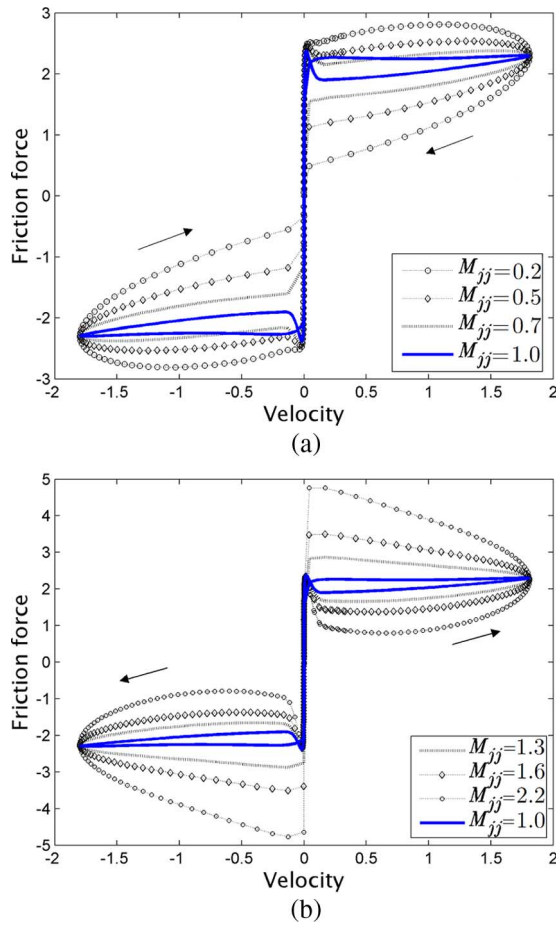

Fig. 2. Effect of mass/inertia perturbation on the friction–velocity graph. (a) Underestimated mass. (b) Overestimated mass.

$\dot{q}_j$ can reduce the measurement errors due to inexact value of M_{jj}. On the other hand, moving a manipulator too slowly does not transition the friction force to the sliding state. Thus, as mentioned earlier, finding an appropriate torque signal for an unknown system requires a few trials. To show the effect of M_{jj} on the friction–velocity graph, a unit mass subjected to an external sinusoidal torque as well as to the friction force was simulated, and the corresponding friction–velocity map was plotted. The friction force was simulated using (2) for the following nominal values: $F_c = 1.2$ N, $F_s = 2.0$ N, $\sigma_0 = 10^3$ N/m, $\sigma_1 = 400$ (N · s)/m, $\sigma_2 = 0.4$ (N · s)/m, $\alpha = 0.2$ s/m, and $M_{jj} = 1$ kg. The simulated values of the friction force were used in the dynamic equations of motion. However, instead of using the same values of the friction force in plotting the friction–velocity map, we recalculated the friction force using (5), similar to a practical case. The results are summarized in Fig. 2. The solid line shows the friction–velocity graph for the nominal values of the parameters, and the dashed lines show the graphs for the perturbed values of M_{jj} from its nominal value.

As can be observed, an incorrect value of M_{jj} cannot only deform the graph, but it can also change the direction in which the graph is followed. It is also clear that both overestimated and underestimated values of M_{jj} can affect the friction–velocity map. In the sequel, parameter identification of the friction model, i.e., identification of F_c, F_s, α, and σ_2, using a friction–velocity map is presented.

B. Measuring σ_0

Let us begin by measuring the value of σ_0 using the results given in [3]. It has been shown that the slope of the friction force–displacement graph while in the presliding state is equal to σ_0 (see for example [3] and [15]). In these references, it has been argued that so long as the two surfaces, which are subjected to an external force, are not freely moving with respect to each other (more precisely the two surfaces are in the presliding state), the fictitious bristles on the two surfaces are only deflected and the friction force–displacement graph is in fact representing the stress–strain graph for the average bristle deflections. Thus, according to the definition of σ_0, the slope of this graph at the origin renders the value of σ_0.

C. Large Values of the Joint Velocity

Considering again a typical friction–velocity map (Fig. 1), the relationship between the model parameters F_c and σ_2, and the graph are discussed next. It is assumed that the average bristle deflections for large values of the joint velocity reach a steady-state value and thus are constant. This is due to the fact that in lubricated contacts, a fluid layer of lubricant is built up at high velocities, and consequently, friction is determined by the viscous characteristics of the lubricants [15]. The small value of the lubricant viscous coefficient suggests that the average deflection of the bristles can be assumed constant, or equivalently, $\dot{z} \simeq 0$. In this case, the friction force is given by

$$0 = \dot{q}_j - \frac{\sigma_0 |\dot{q}_j|}{s(\dot{q}_j)} z \tag{6a}$$

$$\Rightarrow \quad z = \operatorname{sgn}(\dot{q}_j) \frac{s(\dot{q}_j)}{\sigma_0} \tag{6b}$$

$$\Rightarrow \quad \tau_{F_j} = \operatorname{sgn}(\dot{q}_j) s(\dot{q}_j) + \sigma_2 \dot{q}_j. \tag{6c}$$

Without losing generality, let us assume that $\dot{q}_j$ is positive. Additionally, for large values of the joint velocity where $\alpha \dot{q}_j \gg 1$, (3) yields

$$s(\dot{q}_j) = F_c + (F_s - F_c) e^{-\alpha |\dot{q}_j|} \simeq F_c. \tag{7}$$

Now, substituting the value of $s(\dot{q}_j)$ in (6c) from (7) renders the friction force as

$$\tau_{F_j} = F_c + \sigma_2 \dot{q}_j. \tag{8}$$

Thus, for large values of the joint velocity, the friction force is given by a straight line whose slope is equal to σ_2 and its y-intercept is equal to F_c, as illustrated in Fig. 1.

D. Small Values of the Joint Velocity

Considering small values of the joint velocity for which the two conditions of $\alpha \dot{q}_j \ll 1$ and a constant average bristle deflection (i.e., $\dot{z} = 0$) hold will result in

$$\tau_{F_j} \simeq F_s + \sigma_2 \dot{q}_j \simeq F_s. \tag{9}$$

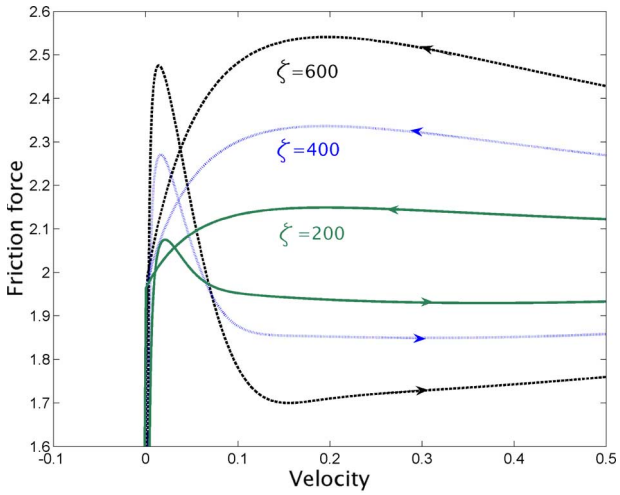

Fig. 3. Transition between the presliding and sliding conditions.

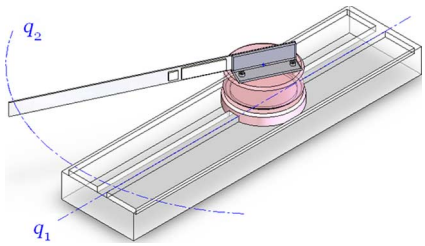

Fig. 4. Two-degree-of-freedom high-speed micromanipulator.

The stated conditions ($\alpha\dot{q}_j \ll 1$ and $\dot{z} = 0$) represent a steady state in the presliding mode, and depending on the system's direction, i.e., leaving or approaching the presliding condition, two different situations can be observed. Let us first qualitatively look at the behavior of the system. Consider the system in the presliding condition. As the velocity increases, so does the value of the friction force. At this so-called elastic stage, the friction behaves similar to a spring. After rupturing this elastic bond, the system enters the sliding mode. Upon transition of the system from the presliding to the sliding condition, because of the assumed friction dynamics, the value of the friction force may exceed the stiction force (static friction) value. This effect is similar to releasing a stretched spring. In this case, the friction–velocity graph, as depicted Fig. 1, has an overshoot. The amplitude of the overshoot depends on the stiffness and damping coefficients, i.e., σ_0 and σ_1, as well as the amplitude of the velocity (input signal of the friction model). On the other hand, prior to approaching the origin of the friction–velocity graph, the system is in the sliding condition, and as a result, the average bristle deflection is relatively constant, i.e., $\dot{z} \simeq 0$ (the assumption made earlier). Hence, the value of the friction force is indeed equal to the stiction force. To quantitatively illustrate this fact, let us consider the linearized model of the system in (2) with the dynamics (4) around the equilibrium point of the system as follows [10]:

$$\frac{q_j(s)}{\tau_j(s)} = \frac{1}{M_{jj}s^2 + (\sigma_1 + \sigma_2)s + \sigma_0}$$
$$\tau_{F_j} = \sigma_0 q_j + (\sigma_1 + \sigma_2)\dot{q}_j, \qquad \dot{q}_j = \dot{z}. \tag{10}$$

TABLE I
FRICTION FORCE PARAMETERS

	F_c	F_s	α	σ_0	σ_1	σ_2
Linear Motor	2.4	4.9	6.7	10^4	500	11.1
Rotary Motor	0.12	0.15	0.1	100	2	0.075

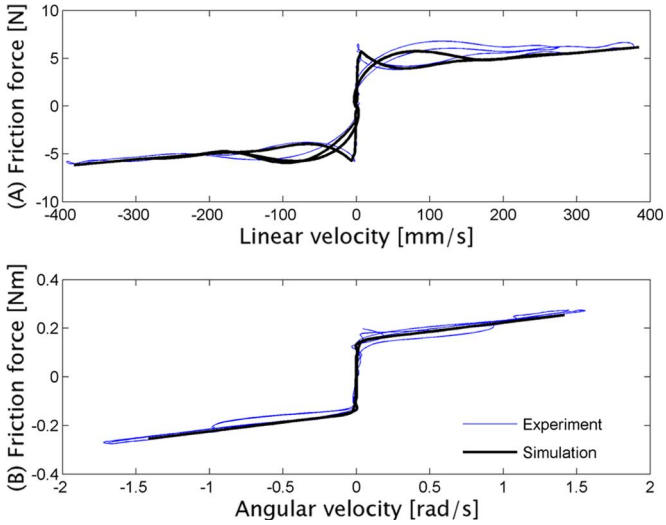

Fig. 5. Simulation and experimental friction–velocity map.

To study the transition of the system from the presliding to the sliding condition and vice versa, the response of the linearized model (10) to the input $\tau_{m_j}\sin(\omega_j t) \simeq A_j t$, where $A_j = \tau_{m_j}\omega_j$, is calculated. It has been shown that the linearized model, despite the nonsmooth behavior of the system at the origin, is valid for both positive and negative velocities [10]. Thus, the complete response of the system is given by

$$q_j(t) = w_j(t) + h_j(t) \tag{11}$$

where $w_j(t)$ and $h_j(t)$ are the zero state and the zero input responses of the system that are given by

$$w_j(t) = K_1 e^{s_1 t} + K_2 e^{s_2 t} + at + b$$
$$h_j(t) = K_3 e^{s_1 t} + K_4 e^{s_2 t}$$
$$s_{1,2} = -\zeta \pm \underbrace{\sqrt{\zeta^2 - \omega_0^2}}_{\omega_d}, \qquad \zeta = \frac{\sigma_1 + \sigma_2}{2M_{jj}}; \qquad \omega_0^2 = \frac{\sigma_0}{M_{jj}}$$
$$K_{1,2} = \pm\frac{A_j}{\omega_0^4}\frac{(\zeta \pm \omega_d)^2}{2\omega_d}, \qquad a = \frac{A_j}{\omega_0^2}; \qquad b = \frac{-2\zeta A_j}{\omega_0^4}$$
$$K_{3,4} = \pm\frac{\dot{q}_j(0) + (\zeta \pm \omega_d)q_j(0)}{2\omega_d}. \tag{12}$$

It is clear that the response of the system in the presliding condition is characterized by the values σ_0, σ_1, σ_2, and M_{jj}. For large values of ζ ($\zeta \gg \omega_0$), the roots of the system, i.e., $s_{1,2}$, tend to be 0_- and $-\infty$, respectively. As a result, q_j, $\dot{q}_j$, and τ_{F_j} that are given in (10) will more gradually approach their final values, i.e., $at + b$, a, and $\sigma_0(at + b) + (\sigma_1 + \sigma_2)a$. Now, depending on the values of $s_{1,2}$, two different situations

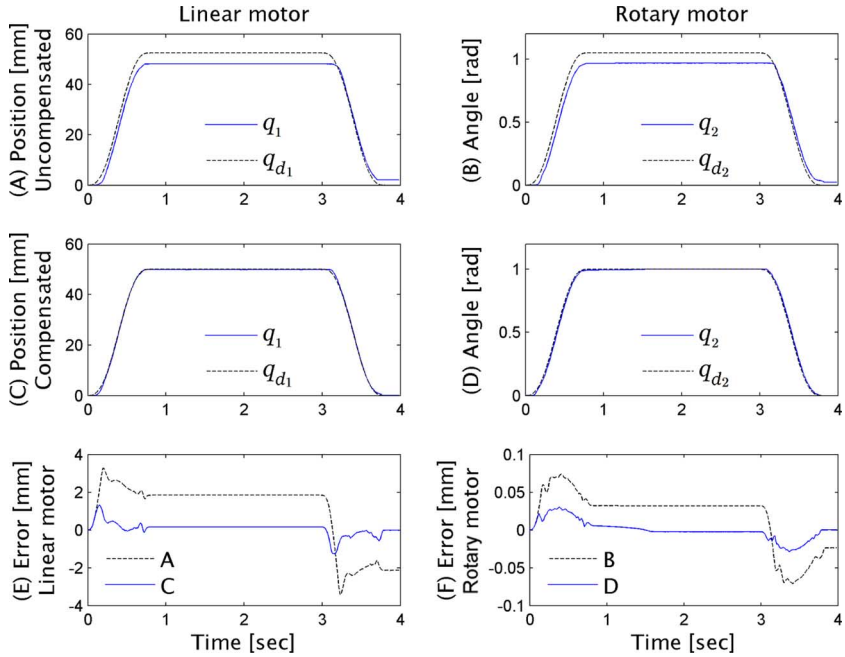

Fig. 6. Tracking performance of linear and rotary motors with and without friction compensation.

are recognizable. Let us denote the time that the input signal reaches F_s as $t_s = (F_s/A_j)$. Calculating τ_{F_j} at t_s yields

$$\tau_{F_j} = \sigma_0 q_j(t_s) + (\sigma_1 + \sigma_2)\dot{q}_j(t_s). \tag{13}$$

Now, if ζ is small enough such that at t_s the exponential terms in the q_j and $\dot{q}_j$ expressions are near zero, then

$$\tau_{F_j} = \sigma_0(at_s + b) + (\sigma_1 + \sigma_2)a. \tag{14}$$

Substituting a and b from (12) in (14) and $t_s = (F_s/A_j)$ yields

$$\tau_{F_j} = F_s.$$

Therefore, upon transition of the system from the presliding to the sliding condition, if ζ is small enough, the friction force is equal to F_s. However, if due to the large values of ζ the exponential terms in q_j and $\dot{q}_j$ are nonzero, then

$$\tau_{F_j} = F_s + \ell$$

where

$$\ell \simeq \sigma_0\left(K_1 e^{s_1 t_s} + K_3 e^{s_1 t_s}\right) + (\sigma_1 + \sigma_2)\left(K_1 s_1 e^{s_1 t_s} + K_3 s_1 e^{s_1 t_s}\right).$$

In this case, the friction force is larger than F_s. The transitions of the friction–velocity graph between the presliding and sliding conditions are depicted in Fig. 3 for three different values of ζ and the nominal values used for plotting Fig. 2.

The aforementioned argument indicates that the value of the friction force in the friction–velocity graph while entering the sliding condition may have an overshoot and thus may be different than the stiction force. The amplitude of the overshoot depends on the values of σ_0, σ_1, and the velocity (input signal). On the other hand, in the sliding condition and just before entering the presliding condition, the low values of the velocity guarantees that the friction force is equal to F_s, as given in (9).

E. Measuring α

To obtain the coefficient α, let us calculate the slope of the friction force graph in the vicinity of the origin. From (6c), we have

$$\frac{\partial \tau_{F_j}}{\partial \dot{q}_j} = -\alpha(F_s - F_c)e^{-\alpha \dot{q}_j} + \sigma_2. \tag{15}$$

Having measured the values of F_s, F_c, and σ_2, α can be obtained from (15) by measuring the slope of the graph near the origin (κ_1 in Fig. 1) as follows:

$$\alpha \simeq -\frac{\kappa_1 - \sigma_2}{F_s - F_c}. \tag{16}$$

In Fig. 3, all three graphs have slope $\kappa_1 \simeq 0$ at $\dot{q}_j = 0.2$, which, using (16), yields $\alpha = 0.5$. Note that finding an exact value of the velocity at which α can be calculated is a tedious task. Having obtained an estimated value of α, the fine tuning of this parameter can be achieved by finding a good match between the friction–velocity map from the model and the measured one.

IV. Case Studies

To evaluate the validity of the results presented in Section III, experiments were performed on two different robotic manipulators. In each case, following the identification of the parameters of the friction model, the closed-loop performance for tracking a desired trajectory using a proportional–derivative (PD) controller was studied.

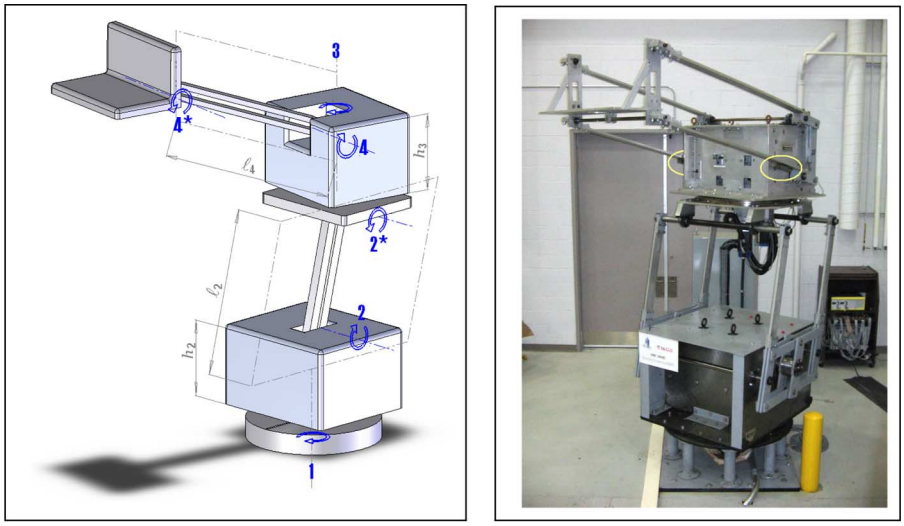

Fig. 7. (a) Schematic of the 4-DOF macromanipulator. (b) Macromanipulator.

A. Micromanipulator

A 2-DOF manipulator, which is used for high-speed and accurate manipulation, was studied (Fig. 4). This manipulator consists of a linear stage carrying a revolute joint (see [13] for details of the micromanipulator). Both joints are actuated with direct drive motors. This makes the identification results more accurate in the sense that no error is introduced in the measurements because of the gearbox. The system has micrometer accuracy and is capable of moving as fast as 1.98 m/s linearly and 2.5 rad/s angularly. The mass and inertia of the linear stage and the revolute joint are known. Moreover, their values do not depend on the manipulator configuration. To identify the friction force at each joint, a sinusoidal signal was applied to one motor, one at a time, while the other motor was locked. Then, a friction–velocity map was obtained for each joint, from which the parameters of the friction force model were extracted as described in Section III. Table I shows the estimated parameters of the friction force for each motor.

The evaluation process of the estimated results included two parts. In the first part, the friction–velocity map from the estimated friction model was compared with that from the experiment. Fig. 5 illustrates the experimental friction–velocity map that is superimposed on its simulation counterpart.

It is clear that despite different friction force characteristics of the two motors, an accurate selection of the model parameters creates an accurate friction–velocity map. It is also worth noting that in cases similar to the rotary motor in which the values of the static and the Coulomb frictions, i.e., F_s and F_c, are close, it is difficult to calculate the value of α from (16). Fortunately, in such cases, incorrect values of α do not affect the results, since the variation of friction force between its two values, i.e., F_s and F_c, is very small.

In the second part, the friction model was evaluated by observing the closed-loop performance of the manipulator for tracking a desired trajectory. In this regard, a PD controller was utilized, and the estimated values of the friction force were added to the control signal to compensate for the actual friction of the system. Fig. 6 compares the experimental results for the position and tracking error of each motor with friction compensation to those without compensation.

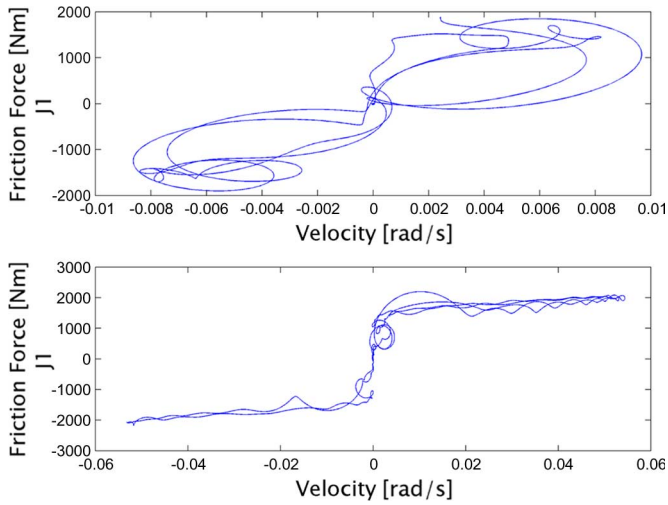

Fig. 8. Friction–velocity map for two velocity levels at joint 1.

TABLE II
FRICTION FORCE PARAMETERS

	F_c	F_s	α	σ_0	σ_1	σ_2
Joint 1	1500	1614	18	10^6	8900	11262
Joint 2	1380	1546	11	10^6	8500	10914
Joint 3	105	116	5	10^5	800	1878
Joint 4	564	610	10	10^5	800	3450

Fig. 6(a) and (c) shows the actual and desired trajectories for the linear motor for the uncompensated and compensated cases, respectively. The error between the desired and actual trajectories for each case is summarized in Fig. 6(e). Fig. 6(b), (d), and (f) shows the same signals for the rotary motor.

B. Macromanipulator

In the second case, a 4-DOF macromanipulator was studied (Fig. 7). Unlike the previous case, the macromanipulator cannot

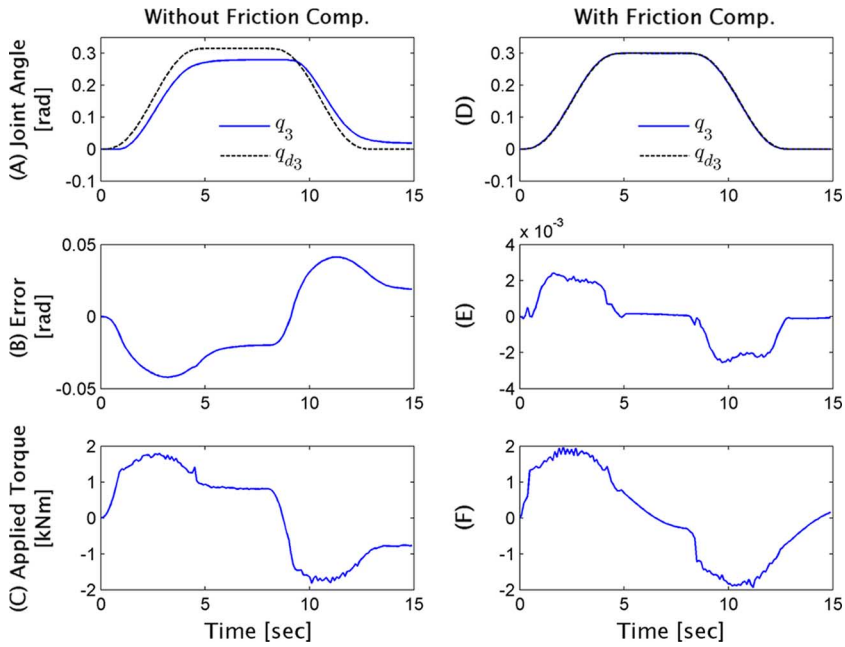

Fig. 9. Joint 3 tracking performance with and without friction compensation.

move fast. It has a much larger load capacity and workspace. The macromanipulator includes two sections, each of which consists of a revolute joint with a vertical axis in series with a $\prod$-joint, producing a 2-DOF motion. The whole system has 4 DOF and is used for positioning a platform at the endpoint of the manipulator. The platform is capable of carrying a load of up to 70 kg (e.g., a PUMA 560). The macromanipulator has a reach of 3.8 m in its fully stretched configuration (see [12] for details). The manipulator is a relatively heavy mechanism, and the maximum speed of its joints are less than 0.4 rad/s. The joints of the manipulator are attached to electric servomotors using gearboxes with gear ratios of J_1 1:489.14, J_2 1:600, J_3 1:310, and J_4 1:324.2, respectively. The presence of gears makes the friction force measurement very difficult. It has been shown that gear transmission systems can be a source of chaotic behavior in multibody systems [16]. In fact, it is not always possible to correctly identify the friction model parameters depending on the severity of the gears' effect. A good understanding of the friction phenomenon helps in achieving reasonably accurate results.

The macromanipulator system is quite different from the previous example. The inertias of the manipulator's links are functions of the joint angles. The joints are under the gravity force. A gear transmission system has been used at each joint. Moreover, at low velocity, the gear pitches show considerable mismatches (backlash), which result in a sudden change of velocity (chaos). At higher velocity, this effect is reduced and allows for measurement of the friction model parameters. The procedure of applying a sinusoidal torque was followed so as to identify the friction force at each joint of the manipulator. Except for α, which specifically requires low velocity information of the system, other parameters were identified using the same methods described previously. The final value of α was selected to produce a good match between the friction–velocity map from experiments and simulations. To show the chaotic effect of the gear, Fig. 8 depicts the friction–velocity map for the first joint for two velocity levels. As observed in Fig. 8(a), the presence of a chaotic behavior on the friction–velocity map of the macromanipulator is noticeable. Note that the first joint of the manipulator is not affected by gravity force and its inertia is independent of other joint angles. The discrepancies between the two graphs are merely due to the gearbox. Yet, by selecting an appropriate input signal, a friction–velocity graph whose parameters are measurable can be obtained. The process was repeated for all four joints. The results of the identification are summarized in Table II.

The closed-loop performance of the manipulator for tracking a desired trajectory was also examined after including the friction model in the control algorithm. A PD controller was utilized for controlling each joint, and in addition to the gravity force, the estimated values of the friction force were added to the control signal. Fig. 9 compares the experimental results for the third joint of the manipulator (a joint with significant friction) in tracking a desired trajectory with and without friction compensation.

V. Conclusion

In this paper, friction compensation in robotic manipulators has been studied. A single-state model of the friction force was utilized, and its parameters were identified. A practical method for measuring the friction force as well as the friction model parameters in a robotic manipulator was discussed. Two different manipulators with different friction characteristics were considered. The estimated results were verified by comparing the estimated friction–velocity map with that experimentally obtained. Moreover, the closed-loop performance of each system for tracking a desired trajectory with and without friction compensation was evaluated. Experimental results showed that including the friction force in the control algorithm significantly

improved the accuracy of manipulation, without sacrificing the speed and smoothness of the manipulation.

REFERENCES

[1] B. Armstrong, P. Dupont, and C. Canudas de Wit, "A survey of models, analysis tools and compensation methods for the control of machines with friction," *Automatica*, vol. 30, no. 7, pp. 1083–1138, Jul. 1994.

[2] N. Barabanov and R. Ortega, "Necessary and sufficient conditions for passivity of the LuGre friction model," *IEEE Trans. Autom. Control*, vol. 45, no. 4, pp. 830–832, Apr. 2000.

[3] P. A. Bliman, "Mathematical study of the Dahl's friction model," *Eur. J. Mech.*, vol. 11, no. 6, pp. 835–848, 1992.

[4] P. A. Bliman and M. Sorine, "A system-theoretic approach of systems with hysteresis, application to friction modeling and compensation," in *Proc. Eur. Control Conf.*, Groningen, The Netherlands, 1993, pp. 1844–1849.

[5] C. Canudas de Wit and P. Lischinsky, "Adaptive friction compensation with partially known dynamic friction model," *Int. J. Adapt. Control Signal Process.*, vol. 11, no. 1, pp. 65–80, 1997.

[6] C. Canudas de Wit, H. Olsson, K. J. Åström, and P. Lischinsky, "A new model for control of systems with friction," *IEEE Trans. Autom. Control*, vol. 40, no. 3, pp. 419–425, Mar. 1995.

[7] P. R. Dahl, "A solid friction model," The Aerosp. Corp., El Segundo, CA, Tech. Rep. TOR-158(3107-18), 1968.

[8] N. E. Leonard and P. Krishnaprasad, "Adaptive friction compensation for bi-directional low-velocity position tracking," in *Proc. 31st Conf. Decision and Control*, Tucson, AZ, 1992, vol. 1, pp. 267–273.

[9] D. Haessing and B. Friedland, "On the modeling and simulation of friction," in *Proc. Amer. Control Conf.*, San Diego, CA, 1990, pp. 1256–1261.

[10] R. H. A. Hensen, M. van de Molengraft, and M. Steinbuch, "Frequency domain identification of dynamic friction model parameters," *IEEE Trans. Control Syst. Technol.*, vol. 10, no. 2, pp. 191–196, Mar. 2002.

[11] R. Kelly, J. Llamas, and R. Campa, "A measurement procedure for viscous and Coulomb friction," *IEEE Trans. Instrum. Meas.*, vol. 49, no. 4, pp. 857–861, Aug. 2000.

[12] M. R. Kermani, R. Patel, and M. Moallem, "Flexure control using piezostack actuators: Design and implementation," *IEEE/ASME Trans. Mechatronics*, vol. 10, no. 2, pp. 181–188, Apr. 2005.

[13] M. R. Kermani, R. V. Patel, and M. Moallem, "Study of system parameters and control design for a flexible manipulator using piezo electric transducers," *Smart Mater. Struct.*, vol. 14, no. 4, pp. 843–849, Aug. 2005.

[14] R. Lozano, B. Brogliato, O. Egeland, and B. Maschke, *Dissipative Systems Analysis and Control, Theory and Applications*. London, U.K.: Springer-Verlag, 2000.

[15] H. Olsson, K. J. Åström, C. Canudas de Wit, M. Gäfvert, and P. Lischinsky, "Friction models and friction compensation," *Eur. J. Control*, vol. 4, no. 3, pp. 176–195, 1998.

[16] F. Pfeiffer, "Unsteady processes in machines," *Chaos*, vol. 4, no. 4, pp. 693–705, Dec. 1994.

[17] J. Swevers, F. Al-Bender, C. G. Ganseman, and T. Prajogo, "An integrated friction model structure with improved presliding behavior for accurate friction compensation," *IEEE Trans. Autom. Control*, vol. 45, no. 4, pp. 675–686, Apr. 2000.

Mehrdad R. Kermani received the B.Sc. degree in electrical and computer engineering from Isfahan University of Technology, Isfahan, Iran, in 1994, the M.Sc. degree in electrical and computer engineering from Iran University of Science and Technology, Tehran, Iran, in 1997, and the Ph.D. degree in electrical and computer engineering from the University of Western Ontario, London, ON, Canada, in 2005.

From 1997 to 2001, he was a Senior Automation Consultant in the steel industry. In 2005, he held a Natural Sciences and Engineering Research Council of Canada Postdoctoral Fellowship at the Canadian Surgical Technologies and Advanced Robotics (CSTAR), University of Western Ontario. He is currently an Assistant Professor with the Department of Electrical and Computer Engineering, University of Western Ontario, and a Scientist with CSTAR. His research interests include vibration control, human-safe robotic systems, smart materials, and mechatronics.

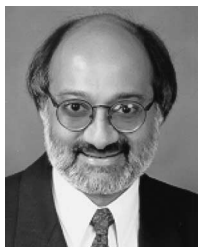

Rajnikant V. Patel (M'76–SM'80–F'92) received the B.Eng. degree (with first class honors) in electronics from the University of Liverpool, Liverpool, U.K., in 1969 and the Ph.D. degree in electrical engineering from the University of Cambridge, Cambridge, U.K., in 1973.

From 1973 to 1998, he held postdoctoral and faculty positions at the University of Cambridge; Lund Institute of Technology, Lund, Sweden; NASA Ames Research Center, Moffett Field, CA; University of Waterloo, Waterloo, ON, Canada; Delft University of Technology, Delft, The Netherlands; Control Systems Centre, University of Manchester Institute of Science and Technology, Manchester, U.K.; and Concordia University, Montreal, QC, Canada. He is currently a Professor and the Tier-1 Canada Research Chair in Advanced Robotics and Control with the Department of Electrical and Computer Engineering, University of Western Ontario, London, ON, and the Director of Engineering of the Canadian Surgical Technologies and Advanced Robotics, London, which is a research initiative of the London Health Sciences Centre. He has coauthored a textbook and five research monographs on robotics and control and coedited an IEEE Press Reprint Book on Numerical Linear Algebra Techniques for Systems and Control.

Dr. Patel is a Fellow of the American Society of Mechanical Engineers. He is currently serving on the editorial boards of the IEEE/ASME TRANSACTIONS ON MECHATRONICS and the IEEE TRANSACTIONS ON ROBOTICS. He is a Registered Professional Engineer in the Province of Ontario.

Mehrdad Moallem (S'95–M'00) received the B.Sc. degree in electrical and computer engineering from Shiraz University, Shiraz, Iran, in 1986, the M.Sc. degree in electrical and computer engineering from Sharif University of Technology, Tehran, Iran, in 1988, and the Ph.D. degree in electrical and computer engineering from Concordia University, Montreal, QC, Canada, in 1997.

From 1997 to 1999, he held postdoctoral and research positions at Concordia University and Duke University, Durham, NC. From 1999 to 2007, he was with the Department of Electrical and Computer Engineering, University of Western Ontario, London, ON, Canada, as an Assistant Professor and then as an Associate Professor. He is currently an Associate Professor with the School of Engineering Science, Simon Fraser University, Burnaby, BC, Canada. His main research interests include real-time and embedded systems, mechatronics, and control applications.